ACS OMEGA

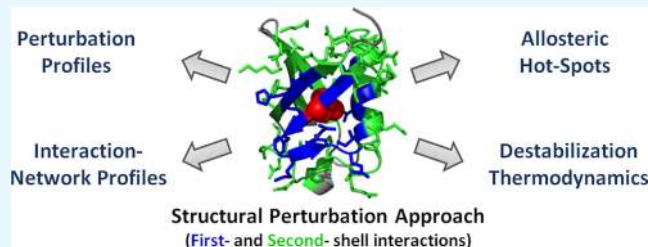Cite This: *ACS Omega* 2020, 5, 1142−1146

Article

pPerturb: A Server for Predicting Long-Distance Energetic Couplings and Mutation-Induced Stability Changes in Proteins via Perturbations

Soundhararajan Gopi,[†] Devanshu Devanshu,[†] Nandakumar Rajasekaran,[†,‡] Sathvik Anantakrishnan,[†] and Athi N. Naganathan*,[†]

[†]Department of Biotechnology, Bhupat and Jyoti Mehta School of Biosciences, Indian Institute of Technology Madras (IITM), Chennai 600036, India

[‡]Department of Biology, Johns Hopkins University, Baltimore, Maryland 21218, United States

ABSTRACT: The strength of intraprotein interactions or contact network is one of the dominant factors determining the thermodynamic stabilities of proteins. The nature and the extent of connectivity of this network also play a role in allosteric signal propagation characteristics upon ligand binding to a protein domain. Here, we develop a server for rapid quantification of the strength of an interaction network by employing an experimentally consistent perturbation approach previously validated against a large data set of 375 mutations in 19 different proteins. The web server can be employed to predict the extent of destabilization of proteins arising from mutations in the protein interior in experimentally relevant units. Moreover, coupling distances—a measure of the extent of percolation on perturbation—and overall perturbation magnitudes are predicted in a residue-specific manner, enabling a first look at the distribution of energetic couplings in a protein or its changes upon ligand binding. We show specific examples of how the server can be employed to probe for the distribution of local stabilities in a protein, to examine changes in side chain orientations or packing before and after ligand binding, and to predict changes in stabilities of proteins upon mutations of buried residues. The web server is freely available at http://pbl.biotech.iitm.ac.in/pPerturb and supports recent versions of all major browsers.

Structural Perturbation Approach
(First- and Second- shell interactions)

INTRODUCTION

The network of noncovalent interactions in the protein interior primarily determines the thermodynamic stability of proteins.[1−3] These evolutionarily fine-tuned intraprotein interaction networks or contact networks display a range of local and nonlocal connectivity, thus determining protein local stability and folding mechanisms. Studies on designed proteins[4] and natural sensory proteins[5] highlight that it is this network of interactions that determines the stability and tunability upon solvent perturbations. Allosteric signals from a perturbation (ligand binding, mutation, and post-translational modification) also propagate through these contact networks, thus determining the functional output.[6−10] In fact, recent works suggest that modulating packing interactions in the protein interior affect the ligand-binding affinity on the protein surface.[11] A central theme in a majority of these approaches is that the interaction network is extremely pliable, contributing to the evolution of proteins, their functionality,[12,13] and cooperativity in protein folding thermodynamics[14,15] and even manifests as disease due to changes in the stability.[16]

Recent works combining graph-theoretic analysis of protein structures, all-atom molecular dynamics (MD) simulations, re-analysis of nuclear magnetic resonance (NMR) experimental data on perturbations point to an intricate connection between the packing density (i.e. the distribution of local and nonlocal interactions) and the extent of percolation of a signal.[9,17−19] They highlight that distance constraints alone can provide a simple avenue to look for allosteric hotspots. The major conclusions of the above work have also been validated through extensive analysis of anisotropic network models[20] and experimental dissection of stability−disease effects in three different proteins.[21] Here, we extend these theoretical results and experimental observations into a web server that can be used to rapidly predict strongly interacting residues, distribution of energetic coupling across the protein structure, and residue-specific parameters that shed light on potential allosteric hotspots and residues that likely determine cooperativity. The server can also be employed to predict the degree of destabilization in proteins upon mutations involving side chain truncation of uncharged residues in the protein interior.
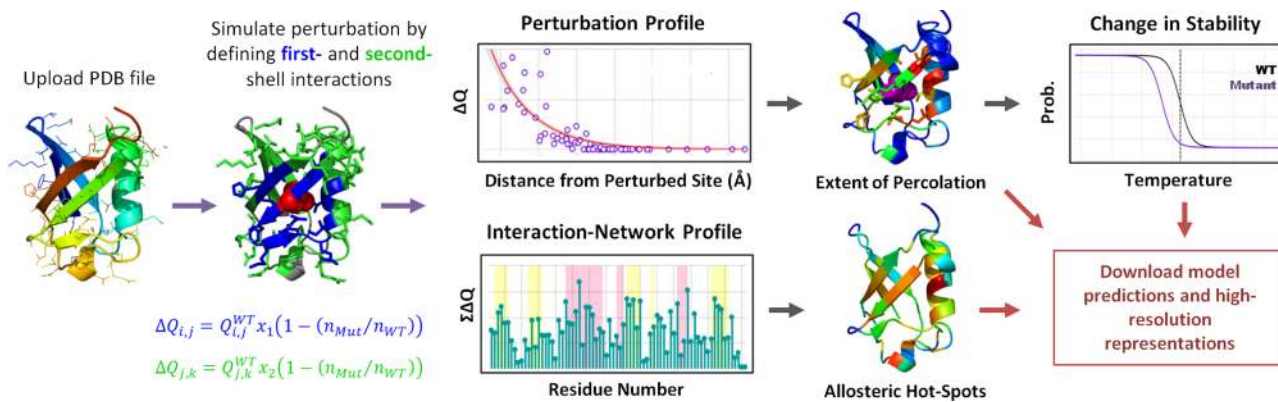
Figure 1. Flowchart depicting the organization of modules in the pPerturb web server. Once the protein structure is loaded into the server, perturbation profiles at the level of individual residues are generated for individual residues using eq 2, following which residue-specific parameters are provided for selected residues (perturbation profile) or all residues in the protein (interaction network profile). The residue-specific parameters are then colored on the protein structure to generate publication-quality images. Users can also request the prediction of changes in stability involving truncation mutations of uncharged residues wherein the mutational effects are introduced via eq 2. The model output can be downloaded as text files or high-resolution images.

■ COMPUTATIONAL METHODS

Perturbation Protocol. Mutations in the interior of a protein are generally assumed to affect only the nearest neighbors (say, within 5−6 Å). However, analysis of MD simulations of several mutants of Ubiquitin suggest that the van der Waals (vdW) packing interactions are distinctly affected at positions 10−15 Å from the perturbed site, and hence the second shell of residues, but decay in an exponential manner.[17] A large-scale analysis of NMR data corroborates simulations and reveals that any mutational perturbation contributes to distinct changes in the chemical shift pattern (and thus the electronic environment) even at residues 10−20 Å from the side of perturbation, following a similar exponential pattern.[18] Inspired by this, we developed a simple relation that connects mutational effects to the strength of packing by recasting the van der Waals interaction energy (E_{vdW}) in terms of the extent to which the first- and second-shell neighbors are affected (x_1 and x_2, respectively) and the nature of the perturbation (i.e., whether V to A or I to A mutation, for example).[17] These statements can be written in the form

$$E_{vdW}^{mut(i,j)} = E_{vdW}^{WT(i,j)}(1 - x_1(1 - n_{mut}/n_{WT}))$$

$$E_{vdW}^{mut(j,k)} = E_{vdW}^{WT(j,k)}(1 - x_2(1 - n_{mut}/n_{WT})) \qquad (1)$$

Here, i is the mutated residue and j and k refer to the first- and second-shell neighbors, respectively. The nature of the perturbation is introduced via n_{mut}/n_{WT}, which corresponds to the ratio of the number of heavy atoms in the mutated residue to that in the wild-type (WT) residue. The van der Waals interaction energy per residue can be estimated either from statistical mechanical models or all-atom MD simulations, as shown before.[17] In this case, values for x_1 and x_2 were estimated by introducing the above relation into the Wako−Saitô−Muñoz−Eaton (WSME) statistical mechanical model[22−24] and varying both the interaction cutoff (4−6 Å for both first and second shells) and the magnitudes of x_1 and x_2 (0−1). By generating more than 100 000 unfolding curves for 375 mutants from 19 different proteins, we arrived at values of 0.5 and 0.2 for x_1 and x_2 (at equal 6 Å radius for first- and second-shell residues), respectively; this involved looking for consistency in three dimensions involving the slope of the plot

of experimental versus predicted change in stability ($\Delta\Delta G$), mean absolute error (MAE), and the correlation coefficient.[17] Equation 1 can also be written in terms of contacts, Q, extracted from the contact map as

$$\Delta Q_{i,j} = Q_{i,j}^{WT}x_1(1 - n_{Mut}/n_{WT})$$

$$\Delta Q_{j,k} = Q_{j,k}^{WT}x_2(1 - n_{Mut}/n_{WT}) \qquad (2)$$

where ΔQ is the extracted perturbation. Equations 1 and 2 are directly related as the van der Waals interaction energy terms in eq 1 can be simply represented as the product of mean-field interaction energy and the number of pairwise atomic-level contacts (Q) between residue pairs and assuming that the mean-field interaction energy itself is not affected by the mutation. A residue-level contact map (Q terms in eq 2) can be constructed by counting the number of heavy-atom interactions between residues within a 6 Å spherical cutoff, which is conventionally done in nearly all Gō-type (native-centric) models of protein folding. This equation alone captures the exponential pattern seen in experiments, thus attesting to its usefulness.[19] Equation 2 can be employed to perform in silico alanine-scanning mutagenesis to probe for the strength of the interaction network across different parts of the protein as recently performed on three proteins implicated in diseases.[21]

Web Server Description. The overall features of the pPerturb web server are depicted in Figure 1. Briefly, the server accepts PDB ID/file as input from the user (protein length, $N \leq 400$) following which it perturbs specific residues or the entire protein based on the experimentally consistent empirical eqs 1 and 2. The perturbation involves truncation of side chains to alanine and in the case of alanine (glycine) to glycine (a virtual three-atom residue) while maintaining two shells of interaction around the perturbed site. The effect of perturbation (written as ΔQ) will be felt at a distance based on the extent to which the perturbed residue is connected to its immediate neighbors or the strength of the interaction network. The ΔQ thus extracted is plotted as a function of distance from the perturbed site and fitted to an exponential function, thus providing an important parameter, the coupling distance, d_C, that captures the extent to which the perturbation

has percolated (in a strict equilibrium sense) into the interaction network. The amplitude of the exponential function and the overall perturbation magnitude ($\sum \Delta Q$) provide additional information on the network features including the magnitude of perturbation and the number of interactions that are perturbed in the immediate neighborhood, respectively.[19] If specific regions of the structure are strongly coupled to each other, then the $\sum \Delta Q$ will be larger and vice versa.[9] The output is generated in a rapid manner; for example, the results for a 400-residue protein can be generated in just ~4 min.

The outputs from the server can be readily accessed as a text file or a graph. In addition to these, we map $\sum \Delta Q$ and/or d_C on to the protein structure, enabling the download of publication-quality images in user-specified orientations, dimensions, and resolutions. These images afford a direct visualization of the residues that are affected upon mutation of a particular residue and can be particularly useful for biologists to understand mutational effects. Users can also input multimeric structures and perturb residues at the interface to explore the nonisotropic percolation of perturbations into the different subunits. It is also possible to compare the changes in intramolecular interaction networks of the same protein at two different states (for example, in the absence and presence of a ligand/cofactor) by uploading the respective protein structures. Following this, the user is given the option of predicting equilibrium unfolding curves from the Wako−Saitô−Muñoz−Eaton (WSME) model assuming an ensemble of 2^N conformational states[22−25] for the truncation mutations involving uncharged residues. This method thus serves as a good starting point for identifying mutations that can precisely alter protein stabilities or to identify regions of structure that primarily contribute to thermodynamic stabilities. For mutations involving charged residues, the user is directed to our pStab web server for predicting changes in stabilities.[26]

■ RESULTS AND DISCUSSION

Visualization of Local Stability or Interaction Network Profiles. We take the challenging case of neurotensin receptor 1 (NTSR1, a G-protein coupled receptor (GPCR)) characterized by seven transmembrane helices (TM1−TM7, Figure 2A). Recent experimental studies point to an activation mechanism involving structural changes in TM5 and TM6.[27] To identify any intrinsic differences in packing density, the perturbation protocol was applied to all residues in the protein and the resulting total perturbation magnitude ($\sum \Delta Q$) was mapped on to the structure. We employ $\sum \Delta Q$ rather than d_C
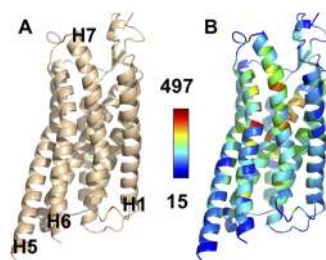

Figure 2. Structural model of GPCR NTSR1 (PDB 6OS9) without (panel A) and with $\sum \Delta Q$ mapped on to the structure (panel B). The structure in panel B is colored in the spectral scale between the two extremes of well-packed residues (red) and weakly packed residues (blue). Note the stretch of dark blue in the TM helices 5 and 6 pointing to weak packing.

as the former does not require recourse to fitting routines, thus reducing any error arising from potential nonexponential decays. The structure is colored in the spectral scale with red and blue representing strong and weak coupling, respectively. It can be seen that the color map of $\sum \Delta Q$ is varied with the majority of the buried residues displaying strong coupling (red to green), while those on the lipid-exposed sites are weakly coupled (blue). Interestingly, we find that TM helices 5 and 6 are weakly coupled to the rest of the structure (not apparent in Figure 2A), thus suggesting that any early structural changes during unfolding or conformational transitions are potentially localized to these regions, in good agreement with experiments.[27]

Structural Changes on Ligand Binding. Many proteins undergo minor or major structural changes on ligand binding, contributing to allosteric effects. Identifying regions that have undergone structural changes requires calculating root-mean-squared deviation (RMSD), a parameter that is agnostic to whether a specific region transitions to a more strongly or weakly packed state on ligand binding. The pPerturb web server provides precisely this information while also accounting for second-shell effects, which we present in Figure 3 in terms of ligand binding to the proteins bACBP, phosphofructokinase (PFK), and PDZ3.[28−30] In each case, we color residues in the spectral scale and depending on whether residues pack stronger (red) or weaker (blue) on ligand binding, as calculated from $\sum \Delta Q_b - \sum \Delta Q_u$, where b and u stand for
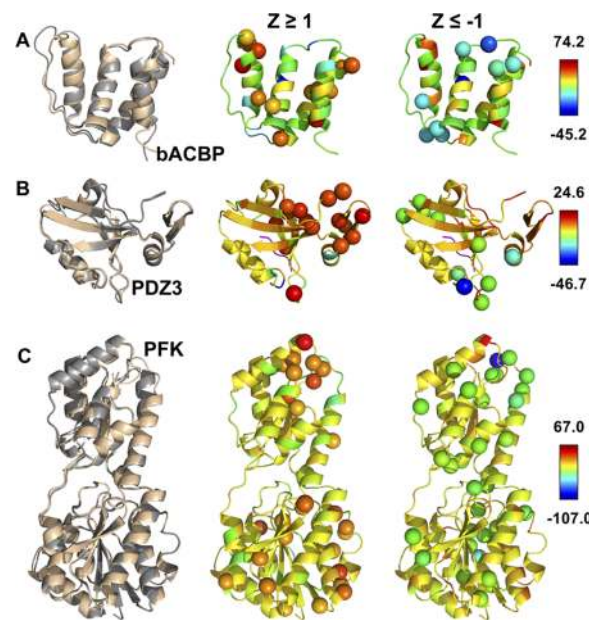

Figure 3. Left column presents a superimposition of ligand/inhibitor-unbound and -bound structures of the proteins bACBP (PDB ids 2ABD/1ACA for ligand-unbound and -bound states), PDZ3 (1BFE/1BE9), and PFK (3PFK/6PFK for inhibitor-unbound and -bound states) in gray and light brown, respectively. The overall RMSD values (including C_α and side chain) between the bound (b) and unbound (u) forms are 2.3, 1.1, and 1.6 Å, respectively. The cartoons in the middle and right columns are colored in the spectral scale (red to blue as in the color bar provided) according to $\sum \Delta Q_b - \sum \Delta Q_u$. Spheres represent the C_α atoms of specific residues whose difference in $\sum \Delta Q$ fall in the extremes, with Z-score ≥ 1 in the middle column and Z-score ≤ −1 in the right column. Note that such vivid details in terms of packing differences (middle and right columns) cannot be extracted from structural superimposition alone (left column).

ligand-bound and -unbound conformations of the protein, respectively. Perturbation analysis shows that that the packing of a large number of residues is affected by ligand binding in all of the three cases considered, in agreement with experiments on PDZ3.[31] In PDZ3, residues that exhibit high $\sum \Delta Q$ difference or Z-scored $\sum \Delta Q$ values greater than 1 highlight a connection between the ligand-binding site (peptide colored in magenta in Figure 3B, middle column) and the phosphorylation site located at the helix-sheet overhang of PDZ3 (residue Y92), exactly as observed in experiments (note the red spheres in Figure 3B, middle column).[32] It is important to emphasize here that our approach does not provide any signal transduction routes but can hint at likely connectivity patterns based on which graph-theoretic tools can be employed to construct signal propagation paths. Moreover, the ligands are not considered in this analysis as ligand binding manifests as changes in packing or coupling, which we extract through perturbation of the conformation that the protein adopts on ligand binding.

Predicting Stability Changes on Truncation Mutations. Since the perturbation protocol relies on modulation of van der Waals interactions, it is straightforward to predict stability changes by introducing eq 1 into the WSME model, as discussed before. We had already shown that the changes in stabilities are predicted with a slope near 1 and a correlation coefficient of 0.7 for a database of 375 mutations.[17] In Figure 4,
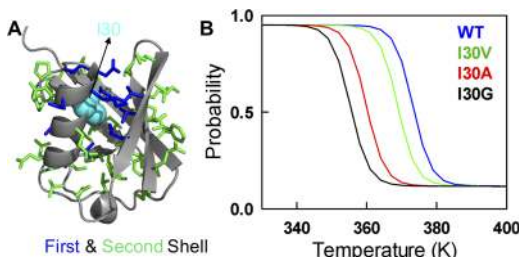

Figure 4. (A) Structure of ubiquitin (1UBQ) highlighting the position of I30 (cyan) together with first- and second-shell neighbors in blue and green, respectively. (B) Unfolding curves predicted by the WSME model for mutations at position 30 at pH 7.0 and 20 mM ionic strength by employing a 6 Å heavy-atom contact cutoff including the nearest neighbors.

we show an illustrative example of the differences in stability arising from progressively weaker packing of I → V → A → G mutations in Ubiquitin. The prediction of the WT and mutant unfolding curves takes just ~2 min in the web server. The protocol involves adjusting the van der Waals interaction energy iteratively to reproduce the experimental melting temperature of the WT at the user-specified pH and ionic strength, following which the perturbation protocol (eq 1) is employed to generate unfolding curves of the mutants. The user is also provided an option of choosing between a uniform entropic penalty for all residues and an entropic penalty that depends on either the residue identity (for glycine and proline) or the presence in a specific secondary structure element (helix and strand versus coil).

CONCLUSIONS

We have developed a multifaceted web server that performs rapid alanine-scanning mutagenesis to probe for the strength of the interaction network accounting for both local and nonlocal interactions in an experimentally consistent manner. The rapidity of the method enables simultaneous prediction of multiple residue-level parameters with implications in identifying pockets of residues that determine local stability and potential allosteric signal transduction paths and in predicting destabilization induced by mutations in the protein interior. The simplicity of our protocol, on the other hand, allows for a tremendous scope in the improvement of the web server to account for residue-specific energy terms and conformational entropy dependent on both the residue identity and secondary structure type.

AUTHOR INFORMATION

Corresponding Author
*E-mail: athi@iitm.ac.in.

ORCID
Soundhararajan Gopi: 0000-0002-7511-2571
Athi N. Naganathan: 0000-0002-1655-7802

Author Contributions
The manuscript was written through the contributions of all authors. All authors have approved the final version of the manuscript.

Notes
The authors declare no competing financial interest.

ABBREVIATIONS USED

WSME, Wako−Saitô−Muñoz−Eaton; NMR, nuclear magnetic resonance; PDB, protein data bank; GPCR, G-protein coupled receptor; MD, molecular dynamics; RMSD, root-mean-squared deviation; vdW, van der Waals

REFERENCES

(1) Baase, W. A.; Eriksson, A. E.; Zhang, X. J.; Heinz, D. W.; Sauer, U.; Blaber, M.; Baldwin, E. P.; Wozniak, J. A.; Matthews, B. W. Dissection of protein structure and folding by directed mutagenesis. *Faraday Discuss.* **1992**, *93*, 173−181.
(2) Eriksson, A. E.; Baase, W. A.; Zhang, X. J.; Heinz, D. W.; Blaber, M.; Baldwin, E. P.; Matthews, B. W. Response of a protein structure to cavity-creating mutations and its relation to the hydrophobic effect. *Science* **1992**, *255*, 178−183.
(3) Rocklin, G. J.; Chidyausiku, T. M.; Goreshnik, I.; Ford, A.; Houliston, S.; Lemak, A.; Carter, L.; Ravichandran, R.; Mulligan, V. K.; Chevalier, A.; Arrowsmith, C. H.; Baker, D. Global analysis of protein folding using massively parallel design, synthesis, and testing. *Science* **2017**, *357*, 168−175.
(4) Boyken, S. E.; Benhaim, M. A.; Busch, F.; Jia, M.; Bick, M. J.; Choi, H.; Klima, J. C.; Chen, Z.; Walkey, C.; Mileant, A.; Sahasrabuddhe, A.; Wei, K. Y.; Hodge, E. A.; Byron, S.; Quijano-Rubio, A.; Sankaran, B.; King, N. P.; Lippincott-Schwartz, J.; Wysocki, V. H.; Lee, K. K.; Baker, D. De novo design of tunable, pH-driven conformational changes. *Science* **2019**, *364*, 658−664.
(5) Narayan, A.; Gopi, S.; Fushman, D.; Naganathan, A. N. A binding cooperativity switch driven by synergistic structural swelling

of an osmo-regulatory protein pair. *Nat. Commun.* **2019**, *10*, No. 1995.

(6) Luque, I.; Leavitt, S. A.; Freire, E. The linkage between protein folding and functional cooperativity: two sides of the same coin? *Annu. Rev. Biophys. Biomol. Struct.* **2002**, *31*, 235−256.

(7) Di Paola, L.; Giuliani, A. Protein contact network topology: a natural language for allostery. *Curr. Opin. Struct. Biol.* **2015**, *31*, 43−48.

(8) Dokholyan, N. V. Controlling Allosteric Networks in Proteins. *Chem. Rev.* **2016**, *116*, 6463−6487.

(9) Naganathan, A. N. Modulation of allosteric coupling by mutations: from protein dynamics and packing to altered native ensembles and function. *Curr. Opin. Struct. Biol.* **2019**, *54*, 1−9.

(10) Guarnera, E.; Berezovsky, I. N. On the perturbation nature of allostery: sites, mutations, and signal modulation. *Curr. Opin. Struct. Biol.* **2019**, *56*, 18−27.

(11) Ben-David, M.; Huang, H.; Sun, M. G. F.; Corbi-Verge, C.; Petsalaki, E.; Liu, K.; Gfeller, D.; Garg, P.; Tempel, W.; Sochirca, I.; Shifman, J. M.; Davidson, A.; Min, J.; Kim, P. M.; Sidhu, S. S. Allosteric Modulation of Binding Specificity by Alternative Packing of Protein Cores. *J. Mol. Biol.* **2019**, *431*, 336−350.

(12) Petrović, D.; Risso, V. A.; Kamerlin, S. C. L.; Sanchez-Ruiz, J. M. Conformational dynamics and enzyme evolution. *J. R. Soc., Interface* **2018**, *15*, No. 20180330.

(13) Tokuriki, N.; Tawfik, D. S. Stability effects of mutations and protein evolvability. *Curr. Opin. Struct. Biol.* **2009**, *19*, 596−604.

(14) Muñoz, V.; Campos, L. A.; Sadqi, M. Limited cooperativity in protein folding. *Curr. Opin. Struct. Biol.* **2016**, *36*, 58−66.

(15) Chan, H. S.; Shimizu, S.; Kaya, H. Cooperativity principles in protein folding. *Methods Enzymol.* **2004**, *380*, 350−379.

(16) Stein, A.; Fowler, D. M.; Hartmann-Petersen, R.; Lindorff-Larsen, K. Biophysical and Mechanistic Models for Disease-Causing Protein Variants. *Trends Biochem. Sci.* **2019**, *44*, 575−588.

(17) Rajasekaran, N.; Suresh, S.; Gopi, S.; Raman, K.; Naganathan, A. N. A general mechanism for the propagation of mutational effects in proteins. *Biochemistry* **2017**, *56*, 294−305.

(18) Rajasekaran, N.; Sekhar, A.; Naganathan, A. N. A Universal Pattern in the Percolation and Dissipation of Protein Structural Perturbations. *J. Phys. Chem. Lett.* **2017**, *8*, 4779−4784.

(19) Rajasekaran, N.; Naganathan, A. N. A self-consistent structural perturbation approach for determining the magnitude and extent of allosteric coupling in proteins. *Biochem. J.* **2017**, *474*, 2379−2388.

(20) Yu, M.; Chen, Y.; Wang, Z. L.; Liu, Z. Fluctuation correlations as major determinants of structure- and dynamics-driven allosteric effects. *Phys. Chem. Chem. Phys.* **2019**, *21*, 5200−5214.

(21) Medina-Carmona, E.; Betancor-Fernández, I.; Santos, J.; Mesa-Torres, N.; Grottelli, S.; Batlle, C.; Naganathan, A. N.; Oppici, E.; Cellini, B.; Ventura, S.; Salido, E.; Pey, A. L. Insight into the specificity and severity of pathogenic mechanisms associated with missense mutations through experimental and structural perturbation analyses. *Hum. Mol. Genet.* **2019**, *28*, 1−15.

(22) Wako, H.; Saitô, N. Statistical Mechanical Theory of Protein Conformation.2. Folding Pathway for Protein. *J. Phys. Soc. Jpn.* **1978**, *44*, 1939−1945.

(23) Muñoz, V.; Eaton, W. A. A simple model for calculating the kinetics of protein folding from three-dimensional structures. *Proc. Natl. Acad. Sci. U.S.A.* **1999**, *96*, 11311−11316.

(24) Naganathan, A. N. Predictions from an Ising-like Statistical Mechanical Model on the Dynamic and Thermodynamic Effects of Protein Surface Electrostatics. *J. Chem. Theory Comput.* **2012**, *8*, 4646−4656.

(25) Naganathan, A. N. A Rapid, Ensemble and Free Energy Based Method for Engineering Protein Stabilities. *J. Phys. Chem. B* **2013**, *117*, 4956−4964.

(26) Gopi, S.; Devanshu, D.; Krishna, P.; Naganathan, A. N. pStab: prediction of stable mutants, unfolding curves, stability maps and protein electrostatic frustration. *Bioinformatics* **2018**, *34*, 875−877.

(27) Kato, H. E.; Zhang, Y.; Hu, H.; Suomivuori, C. M.; Kadji, F. M. N.; Aoki, J.; Krishna Kumar, K.; Fonseca, R.; Hilger, D.; Huang, W.; Latorraca, N. R.; Inoue, A.; Dror, R. O.; Kobilka, B. K.; Skiniotis, G. Conformational transitions of a neurotensin receptor 1-Gi1 complex. *Nature* **2019**, *572*, 80−85.

(28) Kragelund, B. B.; Andersen, K. V.; Madsen, J. C.; Knudsen, J.; Poulsen, F. M. Three-dimensional structure of the complex between acyl-coenzyme A binding protein and palmitoyl-coenzyme A. *J. Mol. Biol.* **1993**, *230*, 1260−1277.

(29) Schirmer, T.; Evans, P. R. Structural basis of the allosteric behaviour of phosphofructokinase. *Nature* **1990**, *343*, 140−145.

(30) Doyle, D. A.; Lee, A.; Lewis, J.; Kim, E.; Sheng, M.; MacKinnon, R. Crystal structures of a complexed and peptide-free membrane protein-binding domain: molecular basis of peptide recognition by PDZ. *Cell* **1996**, *85*, 1067−1076.

(31) Hultqvist, G.; Haq, S. R.; Punekar, A. S.; Chi, C. N.; Engstrom, A.; Bach, A.; Stromgaard, K.; Selmer, M.; Gianni, S.; Jemth, P. Energetic pathway sampling in a protein interaction domain. *Structure* **2013**, *21*, 1193−1202.

(32) Petit, C. M.; Zhang, J.; Sapienza, P. J.; Fuentes, E. J.; Lee, A. L. Hidden dynamic allostery in a PDZ domain. *Proc. Natl. Acad. Sci. U.S.A.* **2009**, *106*, 18249−18254.